Comparative evaluation of phase-change mechanisms for the prediction of flashing flows

I.K. Karathanassis[*1], P. Koukouvinis[1], M. Gavaises[1]

[1]School of Mathematics, Computer Science and Engineering, City, University of London, Northampton Square, EC1V 0HB London, UK

*Corresponding author: Ioannis.Karathanassis@city.ac.uk

Keywords: fuel injectors, two-phase flow, thermodynamic non-equilibrium, kinetic theory of gases, Homogeneous Relaxation Model, bubble dynamics

Abstract. A numerical study is presented, evaluating in a comparative manner the capability of various mass-transfer rate models to predict the evolution of flashing flow in various geometrical configurations. The examined models comprise phase-change mechanisms based on the kinetic theory of gases (Hertz-Knudsen equation), thermodynamic-equilibrium conditions (HEM), bubble-dynamics considerations using the Zwart-Gerber-Belamri model (ZGB), as well as semi-empirical correlations calibrated specifically for flash boiling (HRM). Benchmark geometrical layouts, i.e a converging-diverging nozzle, an abruptly contracting (throttle) nozzle and a highly-pressurized pipe, for which experimental data are available in the literature have been employed for the validation of the numerical predictions. Consideration on additional aspects associated with phase-change processes, such as the distribution of activated nucleation sites, as well as the deviation from thermodynamic-equilibrium conditions have also been taken into account. The numerical results have demonstrated that the onset of flashing flow in all cases is associated with the occurrence of compressible flow phenomena, such as flow choking at the constriction location and expansion downstream, accompanied by the formation of shockwaves. Phase-change models based on the kinetic theory of gases produced more accurate predictions for all the cases investigated, while the validity of the HRM and ZGB models was found to be situational. Furthermore, it has been established that the inter-dependence between intrinsic physical factors associated with flash boiling, such as the nucleation-site density and the phase-change rate, has a significant, yet not clearly distinguishable influence on the two-phase flow characteristics.

Nomenclature

A	area [m^2]
a	volume fraction [-]
c	sonic velocity [m/s]
C_{evap}	empirical coefficient
c_p	specific heat at constant pressure [J/kgK]
c_v	specific heat at constant volume [J/kgK]
D	diffusion coefficient [m^2/s]
F_e	coefficient of the ZGB model
h	specific enthalpy [J/kg]
k	thermal conductivity [W/mK]
Le	Lewis number, $Le = {}^{k}/_{\rho D c_p}$
M	Mach number, $M=u/c$ [-]
N_b	nucleation-site density [sites/m^{-3}]
p	pressure [Pa]
R	evaporation rate [kg/m^3s]
R_b	bubble radius [m]
R_g	ideal gas constant [J/Kmol]
T	temperature [K]
Sc	Schmidt number, $Sc = {}^{\mu}/_{\rho D}$
t	time [s]
u	velocity [m/s]
Y	mass fraction [-]

Greek letters

Θ_r	fraction relaxation time [s]
λ	accommodation coefficient [-]
μ	viscosity [kg/ms]
ρ	density [kg/m^3]

Subscripts/Abbreviations

crit	critical
e	equilibrium
GDI	Gasoline Direct Injection
HK	Hertz-Knudsen
HEM	Homogeneous Equilibrium Model
int	interphase
i	phase
l	liquid
mix	mixture
nuc	nucleation
sat	saturation
sup	superheat
t	turbulent
v	vapour

vof volume fraction

1. Introduction

The main objective of modern engine-components manufacturers is to produce environmentally friendly IC engines, so as to be in compliance with the ever stricter pollutant-emissions legislations imposed globally. Along these lines, significant research effort has been made over the past years for the development of efficient fuel injectors producing an atomized spray of high quality, which, in turn, designates the combustion efficiency. It has been established in the literature that apart from increasing the injection pressure, enhancement of the spray-atomization efficiency can be accomplished by increasing the fuel temperature (Sens et al., 2012). Besides, the topology and evolution of the two-phase jet exiting the injector have been found to be in strong correlation to the in-nozzle flow conditions and primarily to the phase-change rate (Karathanassis et al., 2016). Flash boiling (flashing) is a phase-change process manifested through vapour production due to a rapid liquid depressurization forcing the liquid saturation temperature to values lower than the local liquid temperature; this temperature difference being termed as liquid superheat. The process can be characterized as thermally driven, since the rate of bubble growth is designated by the heat transfer rate at the bubble interface.

There is a significant number of studies available in the literature referring to flashing spray flows. Initial studies, as well as more recent experimental investigations, have employed front or back-lighting projection (shadowgraphy or Schlieren) methods to qualitatively characterize the spray quality (Oza, 1984; Reitz, 1990; Vieira and Simões-Moreira, 2007; Lamanna, 2014). Fundamental studies focusing on identifying the complex flow topology in the near-nozzle region have been performed in simple-orifice geometries and have revealed flow choking at the nozzle outlet and downstream expansion leading to supersonic velocities, increased spray cone angle and formation of shockwaves (Vieira and Simões-Moreira, 2007). The experimental investigation performed by Lamanna et al. (2014) has highlighted that the topology of the spray exiting the nozzle is controlled by bubble nucleation upstream of the nozzle outlet.

Referring to practical applications associated with automotive engineering, the vast majority of experimental studies also focuses on visualizing the external spray region, with the main interest being in GDI-engine injector layouts, which are possible to operate under flash boiling conditions. The high-speed shadowgraphy study of Serras-Pereira et al. (2010) provided simultaneous visualization in the in-nozzle and spray regions of a single-hole injector and demonstrated that lightweight-fuel (gasoline, n-pentane) sprays characterized by a high degree of superheat were found to comprise a high concentration of vapour and fine droplets within the spray. Especially for n-pentane, it was found that the jet emerged already atomized at the nozzle outlet. A subsequent, experimental investigation conducted by Aleiferis and van Romunde (2013) regarding a multi-hole gasoline injector with heated fuel revealed that convergence (collapse) of the different plumes into a single one occurred when the droplet size decreased below 12 μm. Optical, flow-visualization techniques have been widely used for the determination of the macroscopic features of flashing sprays, such as spray-cone angle and tip penetration (Araneo et al., 2000; Mojtabi et al., 2008; Chan 2014). It has been established that onset of flash boiling conditions is associated with reduced spray penetration and increased spray-cone angle.

Further laser-diagnostics studies employing the Laser Induced Exciplex Fluorescence (LIEF) technique, according to which the fluorescence of two laser-excited dyes added to the base fuel is

proportional to the liquid and vapour phase fraction, have been used for the elucidation of flashing sprays, considering the effects of both fuel temperature and ambient pressure (Payri et al., 2006; Zhang et al., 2012; Zeng et al., 2012;). Zhang et al. (2012) reported that for a gasoline surrogate (n-hexane) and a superheat degree of 30K, the LIEF visualization showed significant vapour production in the spray region signifying the plume collapse to a single structure. Zeng et al. (2012), in his LIEF visualization of the spray emerging from a gasoline multi-hole injector distinguished two separate flashing regimes based on the collapse of the different spray plumes. It was concluded that the spray macroscopical features, i.e. penetration and cone angle exhibited inverse trends in the two flashing regimes, i.e. prior and after the collapse of the plumes.

Besides, a number of numerical investigations have been performed regarding flashing flows associated with fuel-injection equipment, with once again the main interest being in externally flashing meta-stable liquid jets. Different phase-change models based on the degree of liquid superheat have been proposed for the vaporization of a flashing spray being expelled into a gaseous environment (see selectively Zuo et al. (2000) and Price et al. (2015)), which have been found to produce accurate predictions regarding the spray macroscopic features, i.e. penetration and plume width. The numerical studies have also confirmed the trend of increased vapour production at elevated fuel temperatures.

On the contrary, limited modelling approaches have been proposed in the literature in reference to geometrically confined flows. Liao and Lucas (2015) modelled the flashing flow in a venturi nozzle, considering that the phase-change rate is dependent on the heat transfer at the bubble interface. Analytical correlations based on the Peclet and Jackob numbers were used for the determination of the local heat transfer coefficient. Schmidt et al. (2010) employed the Homogeneous Relaxation Model (HRM) for the prediction of flashing in steady channel flows. Their numerical predictions showed good agreement with the available experimental results. The HRM model has also been employed in a number of studies to simulate flashing flow in various nozzle geometries and fuels ranging from swirl atomizers to jet-engine applications (Lee et al., 2009; Gopalakrishnan and Schmidt, 2008; Neroorkar et al., 2011). It must be noted that the HRM model has been deemed suitable even for the numerical prediction of cavitating flows due to the similar macroscopic manifestation of the two phenomena (Battistoni et al., 2014). In a recent publication, Saha et al. (2016) coupled the HRM model to the VOF method, in order to predict the in-and near-nozzle two-phase flow evolution of a real GDI injector (Engine Combustion Network, 2014) under realistic operating conditions. The numerical results allowed the distinction of two external vaporization regimes corresponding to flash boiling and convective vaporization owing to the high temperature of the gas medium, where the jet was expelled into.

Although the aforementioned experimental investigations have demonstrated the connection between the in- and near-nozzle two-phase flow, from a numerical perspective, there are only limited studies in the literature elucidating the in-nozzle phase-change mechanism, the factors that have an influence on it, as well as its after-effects on the flow pattern at the near-field region. The present study serves as a comparative evaluation of the predictive capability of various mass-transfer mechanisms (kinetic theory of gases, bubble dynamics, equilibrium and non-equilibrium, semi-empirical) in capturing the phase change in nozzle and pipe flashing flows. Besides, it aims to elucidate the importance of the various model parameters, reflecting intrinsic physical quantities, such as the distribution of nucleation sites or the conditions at the bubble interface, on the designation of the overall phase-change rate. The link between the phase-change rate and the velocity and pressure fields is identified and thoroughly explained, allowing the

justification of distinct flow phenomena associated with flashing flows, including, increase of the spray-cone angle and formation of shockwaves. The formulation of the numerical models is discussed in detail in the next section, followed by the presentation of the numerical predictions. The main findings of the study are summarized in the conclusions section.

2. Description of the cases investigated

2.1 Benchmark geometries and operating conditions

Three geometrical arrangements have been selected for performing numerical simulations. The relatively simple geometries used ensure that no significant flow perturbations induced by the geometrical layout will set in. In addition, experimental data are available for all the cases examined, allowing the verification of the numerical-predictions validity. More specifically, the benchmark geometries comprise a convergent-divergent nozzle ("Moby Dick" nozzle) (Asaka, 1992; Staedtke, 2006), a throttle-nozzle with an abrupt decrease of its cross section used in the experimental investigation of Reitz (1990), as well as a highly-pressurized pipe (Edwards' blow-down pipe) (Edwards and O'Brien, 1970). In terms of flow conditions, the first two cases constitute steady inlet-outlet flows, while in the "Edwards' pipe" case, the phase-change process is transient and leads to full vaporization of the liquid. Water was used as the working medium in all configurations with variable thermophysical properties calculated through the respective values available in the IAPWS tables (Wagner and Pruss, 2002).

The total length of the "Moby Dick" nozzle, shown in **Fig. 1a**, is approximately equal to 1.0m and comprises a convergent section, a long cylindrical throat and a divergent section with an angle of aperture of 7◦. The nozzle is operating with inlet and outlet pressures equal to 20.0bar and 5.0bar respectively, with the liquid temperature at the inlet being 2.0 K lower than the saturation temperature for the prevailing pressure. The "Reitz" nozzle depicted in **Fig. 1b** realizes a step-wise flow contraction with a blockage ratio (D_{down}/D_{up}) of 4.65, whereas the nozzle length to diameter ratio is equal to 4. A constant pressure equal to 7.88bar, is set at the nozzle inlet, while the flow discharge is straight to the environment. Different test-cases were examined by Reitz (1990) with the liquid temperature being in the range 360-427K. **Fig. 1c** depicts the schematic representing the "Edwards' pipe", a duct with a length of approximately 4.0m containing water pressurized at 7.0MPa through a disc placed at its outlet and temperature of 502K. The transient blow-down is initiated by the rupture of the disk allowing the rapid discharge to the environment at atmospheric pressure.

2.2 Computational domains and governing equations

Since all the nozzle layouts considered are axisymmetric, two-dimensional domains were deemed as representative of the actual geometries and were used for the simulations (**Fig. 1**). It must be noted that the domains were extended and appropriate volumes were placed at the outlet regions of the "Reitz" and "Edwards" cases, so that boundary conditions are not placed in regions, where high gradients are expected to occur and, furthermore, to allow the un-perturbed evolution of the jet cone downstream the geometrical constriction. Domain discretization was performed using primarily structured grids, as also depicted in **Fig. 1**. Telescopic, local grid refinement methodology allowed the creation of a fine grid in the regions, where complex flow phenomena are expected to occur, e.g. at the regions of flow contraction/expansion.

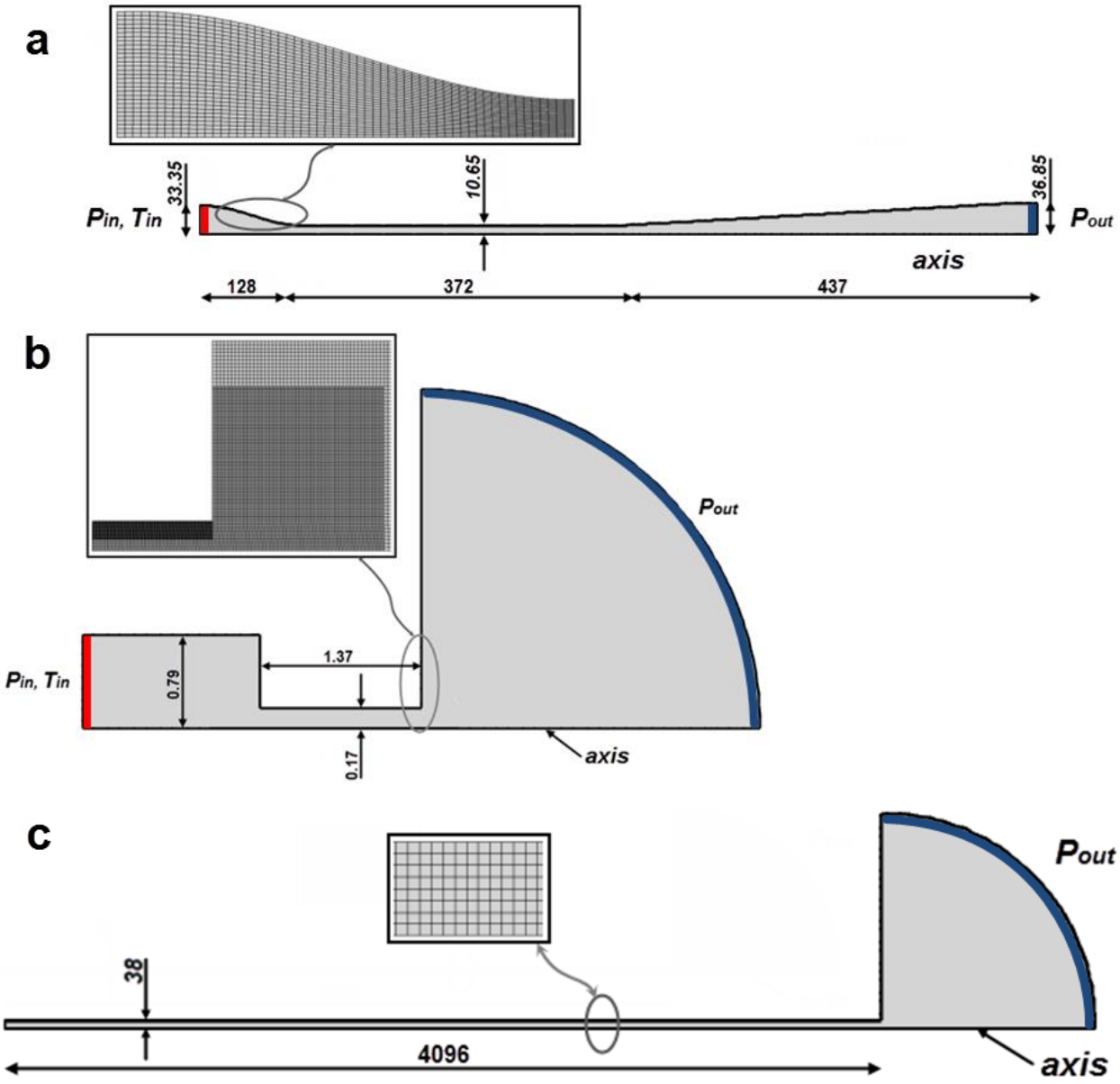

Figure 1. Computational domain and grid topology (all dimensions in mm): (a) "Moby Dick" nozzle, (b) "Reitz" nozzle, (c) "Edwards' pipe".

A two-phase mixture model was employed in order to capture phase-change effects with a common velocity field assumed for the two phases (mechanical-equilibrium assumption). The liquid phase was treated as compressible (Tait equation of state), while the respective vapour phase was considered an ideal gas. The set of governing equations comprised the continuity, momentum and energy equations for the two-phase mixture (ANSYS FLUENT, 2012), as well as an additional advection equation corresponding to the conservation of the secondary phase, i.e. the vapour, volume fraction *a*:

$$\frac{\partial(\rho_{mix})}{\partial t}+\nabla(\rho_{mix}\vec{u})=0 \qquad \textit{(continuity)} \qquad (1a)$$

$$\frac{\partial(\rho_{mix}\vec{u})}{\partial t}+\nabla(\rho_{mix}\vec{u}\vec{u})=-\nabla p+\nabla\left[\mu_{mix}\left(\nabla\vec{u}+\nabla\vec{u}^{T}\right)\right] \qquad \textit{(momentum)} \qquad (1b)$$

$$\frac{\partial}{\partial t}\sum_{i=1}^{2}\left(a_i\rho_i \mathrm{E}_i\right)+\nabla\sum_{i=1}^{2}\left(a_i\vec{\mathrm{u}}\left(\rho_i \mathrm{E}_i+p\right)\right)=\nabla\left(k_{mix}\nabla T\right),\quad E_i=h_i-\frac{p}{\rho_i}+\frac{u_i^2}{2} \qquad \textit{(energy)} \qquad (1c)$$

$$\frac{\partial(a\rho_v)}{\partial t}+\nabla(a\rho_v\vec{\mathrm{u}})=\dot{R} \qquad \textit{(vapour volume fraction)} \qquad (1d)$$

where the indices *mix* and *i* correspond to the mixture and each separate phase. Referring to **Eqs. (1a)-(1d)** ρ, h, α, $\vec{u}$, $\dot{R}$ correspond to density, sensible enthalpy, vapour volume fraction, velocity field and vaporization mass-transfer rate. Especially referring to the energy **Eq. (1c),** further details on the definition of the internal energy and the numerical manipulation performed by the commercial solver can be found in (ANSYS FLUENT, 2012). The modelling approach according to which an additional vapour volume-fraction conservation equation, **Eq. (1d)**, is solved, with a source term added to its right-hand side to account for liquid vaporization constitutes common practice in reference to two-phase flows (see selectively, Magnini and Pulvirenti, 2011; Lee et al., 2009; Janet et al., 2015; Ji et al., 2014; Yan et al., 2001; Žnidarčič et al., 2015). The addition of a diffusion term of the form $\left(\rho D+\frac{\mu_t}{Sc}\right)\nabla Y$ on the right-hand side of **Eq. (1d)** has been verified through preliminary simulations performed for the Moby-Dick case, assuming a constant, approximate value for the diffusion coefficient $D(=k/\rho c_p\approx 10^{-7}$ m^2/s, i.e., *Le=1*) and *Sc=0.7*, to have a negligible effect on the produced numerical results. Hence, taking into account that the main objective of the present study is to compare different phase-change rates for flashing flows, and that data are not available for *D* in reference to such flows, **Eq. (1d)** has been employed in the presented form. Yet depending on the prevailing flow conditions, the effect of the diffusion term could be significant and should not be omitted referring to other two-phase flows not relevant to this study.

It must be pointed out that contributions to the mixture viscosity μ_{mix} and thermal conductivity k_{mix} are made by terms specified using the k-ω SST model to account for turbulence effects, as the nominal Reynolds-number values characterizing the flow in the "Moby Dick", "Reitz" and "Edwards' pipe" cases are in the order of $4.0\cdot10^6$, 62000 and, 10^7 respectively, which are well within the turbulent regime. The SST k-ω model was selected to capture turbulence effects, as it has been demonstrated to be performing well to both moderately and highly turbulent flows, and furthermore it is recommended for flows where recirculation is possible to set in, e.g. throttle flows (Menter, 2012).

As also depicted in **Fig. 1**, suitable boundary conditions were supplied for the governing equations, in order to numerically replicate the flow conditions prevailing during the respective experimental investigations. Constant pressure values, equal to the operating ones set during the experiments, where imposed at the domain inlet and outlet for the "Moby Dick" and "Reitz"

computational domains. A constant inlet temperature of 483.5K was set for the "Moby Dick" nozzle, while inlet temperatures in the range 400-427K, as onset of flash boiling was detected for the specific range, were set for the different test cases examined for the "Reitz" nozzle. Regarding the "Edwards' pipe" domain, a constant atmospheric pressure was imposed at the outlet, i.e. at the edge of the quarter-circular plume. All the other outer edges of all three domains, apart from the axis of rotation, were treated as walls and the no-slip condition was imposed.

The "Moby Dick" and "Reitz" simulations were initialized assuming pure liquid in the entire domain, while the pressure was set equal to the inlet pressure. Especially for the HRM (see section 2.3), where a non-zero value of a is required for phase change to commence, initial values of $p=p_{out}$ and $a=1$ were patched at the expanding parts of the aforementioned domains, since preliminary simulations verified full vaporization and depressurization of the liquid at those regions. For the "Edwards' pipe" case, in order the transient phenomenon to commence pure liquid ($a=0$) must be assumed within the duct ($X<4096mm$) and pure vapour (a=1) at the duct outlet and downstream ($X\geq4096mm$). Calculations for the first two cases were carried out until it was confirmed that a steady solution had been reached and it was verified that a flow time of 2.5 ms was sufficient for both cases. The simulation was declared as complete for the "Edwards' pipe" case after a total flow time of 0.5s for which the entire liquid within the duct had been fully vaporized.

The coupled pressure/velocity, implicit solver implemented in FLUENT (v. 14.5) (2012) was used, with second order schemes for turbulence advection and momentum. The capability of coupled solvers to predict compressible/shockwave flows has been demonstrated in the literature, see selectively (Demirdžić et al., 1993; Chen and Przekwas, 2010; Koukouvinis and Gavaises, 2015). The transient solver was employed with a time step of $1\cdot10^{-6}$s, which produced values of the Courant–Friedrichs–Lewy (CFL) condition less than 15 for all cases that can be easily handled by the implicit solver. It must be noted that 15 corresponds to the maximum cell CFL value obtained for all the cases examined. The specific value occurred at the throttle region of the "Reitz" configuration where the grid is very fine (see **Fig. 1b**) and high flow velocities occur. However, the flow in both the "Moby Dick" and "Reitz" cases converges to steady-state solutions, and hence relatively high CFL values do not interfere with the solver capability of capturing phenomena associated with compressible flow, such as shockwaves, the occurrence location of which remains static and time-invariant in the aforementioned cases. Referring to the "Edwards' pipe" layout, where the flow is transient, the time step has been properly adjusted, so as the Courant number not to exceed a value of 0.8 throughout the evolution of the solution. Although, the flow reaches a steady-state solution in the "Moby Dick" and Reitz cases, yet the transient solver was employed in order to improve the convergence of the solution.

2.3 Two-phase/Mass-transfer models

From a flow physics point of view, the discrimination between equilibrium and non-equilibrium conditions refers to the temperature distribution locally at the interface between the growing bubble and the surrounding interface. At equilibrium conditions, a thermal boundary layer of non-negligible thickness (see **Fig. 2a**) surrounds the bubble interface and hence the liquid and vapour temperature on each side of it are postulated as equal. Consequently, heat transfer rate is infinite and the phase-change process is governed by inertia. On the contrary, for non-equilibrium conditions (**Fig. 2b**) the boundary layer thickness is taken as infinitesimally

small and a temperature discontinuity occurs at the interface. In that case, the bubble-interface velocity and consequently the phase-change rate are strongly linked to the finite local heat transfer rate designated by the respective temperature gradient.

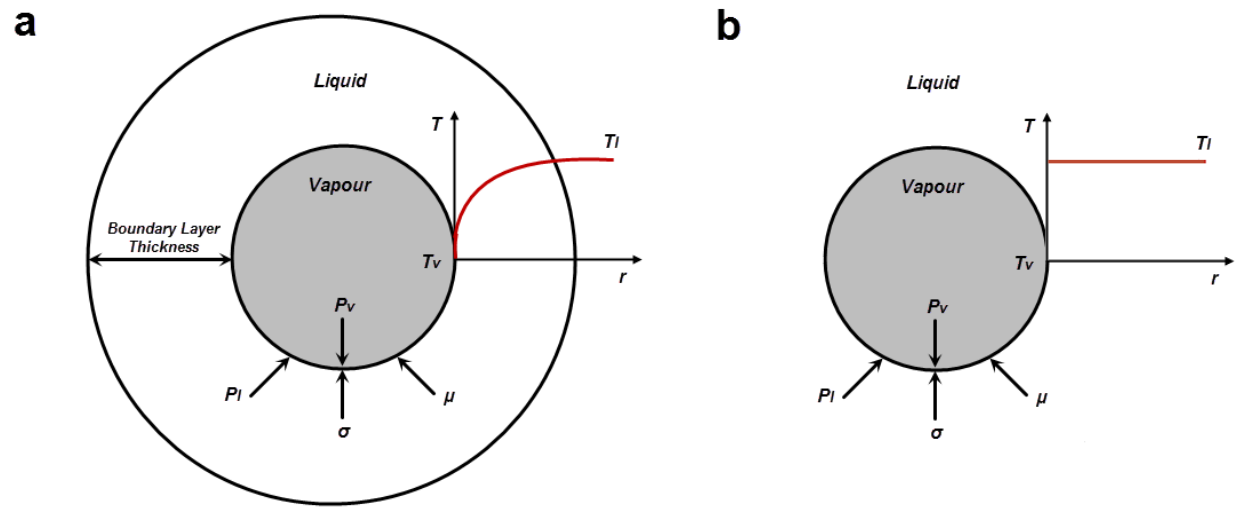

Figure 2. Schematic of growing bubble and surrounding liquid for thermodynamic (a) equilibrium and (b) non-equilibrium conditions.

In the framework of the present investigation, a number of approaches were considered for modelling the mass-transfer rate term of **Eq. (1c)** by also taking into account non-equilibrium phenomena. The phase-change models formulated in this section were implemented in the solver as User Defined Functions (UDFs). Firstly, a generalized mass-transfer rate derived from kinetic theory of gases and similar to the initial correlation proposed by Knudsen (1915) has been tested:

$$\dot{R} = C_{evap} A_{int} a_l \rho_l \left(p_{sat} - p \right) \tag{2}$$

where a_l and ρ_l are the liquid volume fraction and density, respectively, while C_{evap} is an empirical coefficient. A correction has been made to the saturation pressure, namely $p_{sat} = p_{sat}(T) + \frac{1}{2}(0.39k\rho)$, with k being the turbulent kinetic energy, in order to take into account the effect of turbulence on cavitation inception as reported, for instance by Singhal et al. (2002). The mentioned correction has been applied to all two-phase models. A_{int} is the overall bubble-cloud interphase surface area, which is calculated assuming a nucleation-site density of 10^{13} sites/m^3 and a bubble radius of 10^{-6} m. It has to be pointed out that, since the mixture model is employed, the bubble interface is not captured and therefore the bubble-cloud distribution is, in essence, a "lumped" parameter employed for the determination of the overall phase-change rate. The assignment of a constant distribution of vapour bubbles, of course, constitutes an approximation, however it is essential to bear in mind that contaminants, micro-bubbles or impurities, in the bulk of the liquid act as potential nucleation sites and hence the determination of the actual distribution is actually case dependent. It has been verified by different water-tunnel experiments that the nucleation-site density in the case of cavitating flow lies within the range

10^{12}-10^{13} sites/m^3 for vapour bubbles having radii less than 10μm, as summarized by Brennen (1995). The measurements of Ceccio (1990) regarding cavitation development over a benchmark protrusion also verified a site density approximately equal to 10^{12} for bubbles with radii of 10μm. Zwart et al. (2004) have calibrated their phase-change model at several benchmark cases and deduced that a bubble radius of 1μm offers the best matching to available experimental data. To the authors' knowledge there are no data for the nucleation site distribution available in the literature, in reference specifically to flashing flows. However, estimations derived through numerical models are in the range of 10^9-10^{11} sites/m^3 considering bubble radii of the order of 10μm (Riznic and Ishii, 1989; Shin and Jones, 1993). Based on the above, a distribution of 10^{13} bubbles per m^3 of liquid with radii of 1 μm has been adopted in the present study, which produces an overall interphase surface area comparable to the available data for both cavitating and flashing flows, while also the bubble-radius value employed is in compliance with that suggested by Zwart et al. (2004).

A variation of the Hertz-Knudsen equation (Fuster et al., 2010), where deviation from thermodynamic-equilibrium conditions is taken into account through an accommodation coefficient λ, has also been considered:

$$\dot{R} = \frac{\lambda A_{int}\left(p_{sat} - p\right)}{\sqrt{2\pi R_g T_{int}}} \tag{3}$$

where R_g and T_{int} are the ideal gas constant and the temperature at the bubble interphase, respectively. As has been already discussed, an interphase-capturing technique is not employed in the present study; consequently, the interphase temperature is taken as equal to the local cell temperature, which is calculated by the solution of the energy equation. A value of unity for the λ coefficient corresponds to a heat-transfer rate at the bubble interphase approaching infinity and thus thermodynamic-equilibrium conditions. On the contrary, a value of 0.1 or lower suggests a significant deviation from equilibrium (Brennen, 1995). A different formulation of Eq. (3) where a temperature discontinuity is assumed at the bubble interface, as proposed by Theofanous et al. (1969), has also been considered:

$$\dot{R} = \frac{\lambda A_{int}}{\sqrt{2\pi R_g}}\left(\frac{p_{sat}}{\sqrt{T_l}} - \frac{p}{\sqrt{T_v}}\right) \tag{4}$$

with T_l and T_v being the local liquid and vapour temperature, respectively, with the latter being taken equal to the saturation temperature for the local pressure.

The Homogeneous Relaxation Model (HRM) (Bilicki and Kestin, 1990) has also been proposed as suitable for the prediction of flashing flow and is based on the concept that thermal equilibrium between the liquid and vapour phases establishes after the passage of a characteristic time interval referred to as fraction relaxation time Θ_r given by the following relation:

$$\Theta_r = \Theta\, a^m \phi^n \tag{5}$$

where Θ is a semi-empirical timescale, m and n are fitting coefficients, a is the vapour volume fraction and φ is a non-dimensional pressure difference defined as:

$$\phi = \left| \frac{p_{sat} - p}{p_{sat}} \right| \tag{6a}$$

for pressures below 10 bar, whereas for pressures exceeding that value, the following correlation has been proposed:

$$\phi = \left| \frac{p_{sat} - p}{p_{crit} - p_{sat}} \right| \tag{6b}$$

Indicative values for Θ_0, m and n, as reported by Schmidt et al. (2010), are $6.51 \cdot 10^{-4}$ s, -0.257, and -2.24, for the "low pressure" formulation of the model ($p<10$ *bar*), whereas for the respective "high-pressure" variation, the corresponding values are $3.84 \cdot 10^{-7}$ s, -0.54, and -1.76. The mass-transfer rate then results as:

$$\dot{R} = -\rho_{mix} \frac{Y - Y_e}{\Theta} \tag{7}$$

where ρ_{mix} is the mixture density and Y_e is the thermal-equilibrium mass fraction calculated using the following relation:

$$Y_e = \frac{h_{mix} - h_{sat,l}}{h_{sat,v} - h_{sat,l}} \tag{8}$$

where h_{mix} corresponds to the mixture specific enthalpy, while $h_{sat,v}$, $h_{sat,l}$ are the vapour and liquid specific enthalpies at saturated conditions.

Finally, considering that cavitation and flash boiling could be characterized as processes of similar nature, since both are manifested through bubble nucleation caused by a rapid depressurization process, a bubble-dynamics model has also been taken into account for the present investigation. The model proposed by Zwart et al. (ZGB model) (2004) is based on the solution of a simplified form of the Rayleigh-Plesset equation, where the higher order, viscosity surface tension and gas content terms are neglected. Semi-empirical parameters are also employed by the model in order the mass-transfer rate to be derived:

$$\dot{R} = F_e \frac{3 a_{nuc} a_l}{R_b} \sqrt{\frac{2}{3\rho_l} \left(p_{sat} - p \right)} \tag{9}$$

where F_e is a model empirical constant and a_{nuc} is the nucleation-site volume fraction. These model constants have typical values of 50 and 0.0005, respectively, as suggested by Zwart et al. (2004) for the case of cavitation. R_b is an estimation of the mean-bubble diameter, which is in essence a model tuning parameter explicitly correlated to the nucleation-site density, as dictated by the formulation of the ZGB model. Besides, it must be noted that since, at flash boiling

conditions, no vapour condensation takes place, the phase-change term $\dot{R}$ is activated when the pressure-difference term in the square root of Eq. (9) becomes positive, while the same applies for the respective terms of all models.

It is important to point out that the modelling approaches examined apart from the HRM require the estimation of the density and distribution of activated nucleation sites for the derivation of the mass-transfer rate. In fact, it has been verified that the mass-transfer rate associated to flash boiling is significantly enhanced by the activation of additional nucleation sites (Lamanna et al., 2014). In the cases examined in this study, it has been assumed that the nucleation-site density is constant and equal to 10^{13} sites uniformly distributed per unit of the liquid volume for the reasons that have already been reported in the discussion regarding the derivation of **Eq. (2)**. In order to highlight the effect of the nucleation-site density on the produced results, a correlation of the site-density N_b with the degree of superheat ΔT_{sup} proposed by Senda and Hoyjo (1994) has also been considered, as follows:

$$N_b = C_n \, exp\left(\frac{-5.279}{\Delta T_{sup}}\right) \tag{10}$$

where C_n corresponds to the number of maximum available nucleation sites and is taken equal to 10^{13}.

2.4 Homogeneous Equilibrium Model (HEM)

A numerical formulation of different principle, where a vapour fraction equation is not solved, has also been considered in this study. The specific phase-change model is based on the assumption of thermodynamic-equilibrium between the liquid/vapour phases, rendering the mass-transfer rate at the bubble interface as infinite. Thus, an appropriate Equation of State (EOS) directly linking pressure to density has been applied in order to describe the phase-change process. The Tait EoS was employed for the liquid phase, while the vapour phase was assumed an ideal gas. Referring to the mixture, the liquid/vapour phases were assumed to be in thermal and mechanical equilibrium, while the pressure was taken to be equal to the saturation pressure (Koop, 2008). The set of governing equations comprised the Navier-Stokes and energy equations, solved for the homogenous fluid mixture of the liquid and vapour phases.

2.5. Grid-independence study

The sensitivity of the produced results to the grid resolution has been test for all the cases examined by monitoring the effect of the grid density on the numerical results. The Hertz-Knudsen model, **Eq. (3)**, was indicatively selected to model phase-change and consecutive tests with computational grids of increasing density were performed for all cases. The grid topology in reference to the three geometrical layouts can also be seen in **Fig. 1**. Vapour volume fraction distributions were monitored at characteristic locations for each layout to judge on the grid independence of the solution, since the phase-change rate influences the pressure, velocity and temperature fields.

A total number of 15240, 20042 and 16288 grid cells were found to be sufficient for producing accurate results, in respect to the "Moby Dick", "Reitz" and "Edwards'" cases, respectively. Indicatively, referring to the regions of interest, in the "Moby Dick" case, the straight nozzle part was discretized with a cartesian grid of 28 (half cross-section) x 214 (length) cells. Likewise, the throttle region of the "Reitz" nozzle with a grid of 30 x 274 cells and the duct region of the "Edwards' pipe" case by 8 x 819 cells, respectively. As shown in **Fig. 3,** further grid refinement had a negligible effect on the vapour fraction distribution for all cases. More specifically, the average vapour volume-fraction value at the wall of the straight nozzle section, as produced by a refined grid of 31596 elements for the Moby-Dick case (**Fig. 3a**), varied by 0.6% compared to the respective value produced by a 15240-element grid. Refining the grid for the "Reitz" nozzle (**Fig. 3b**) from 20042 to 41615 elements resulted to a variation of less than 0.7% in the average vapour fraction value at the throttle wall (Y=0.00017). Likewise, referring to the "Edwards' pipe" case (**Fig. 3c**), a grid refinement from 16288 to 35535 elements lead to a discrepancy in the order of 0.2% in the average value of the vapour volume fraction at the duct wall (X=0.038m).

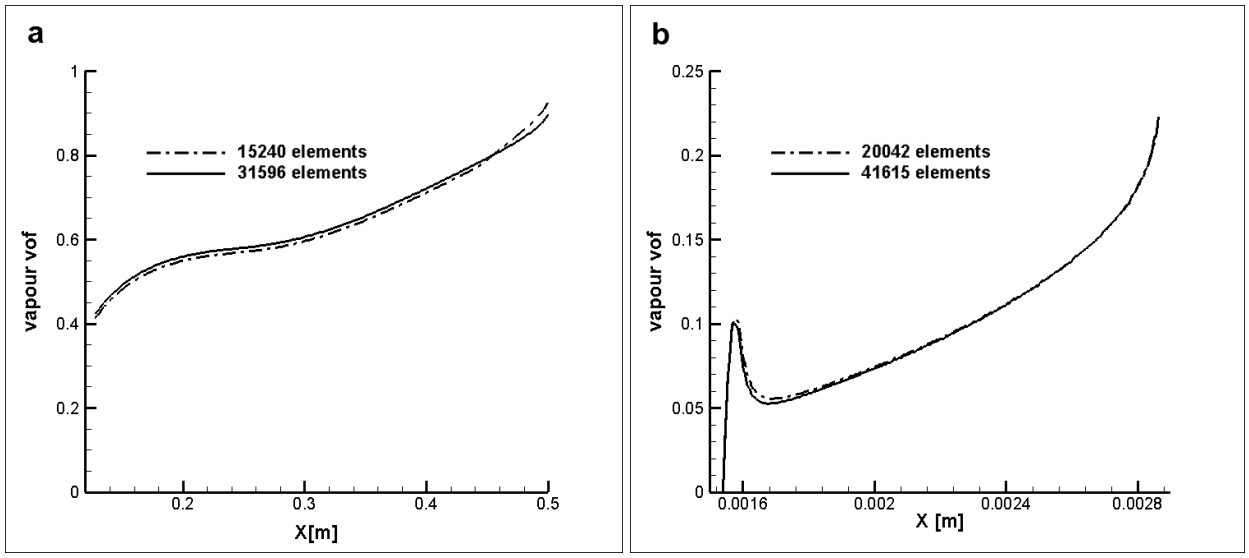

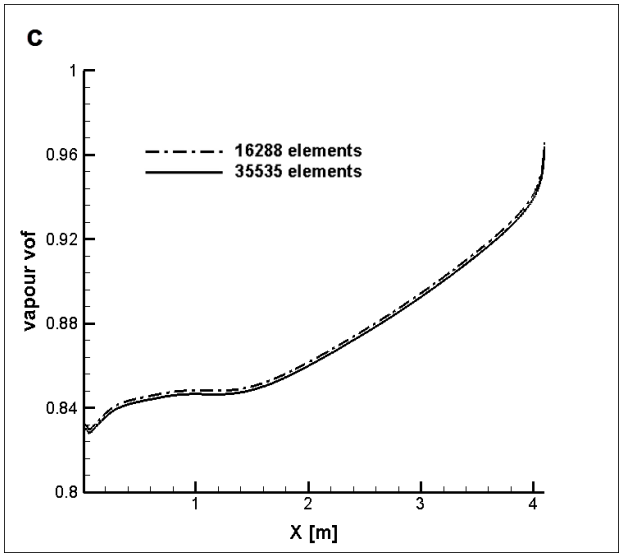

Figure 3. Effect of the grid density on the vapour volume fraction distribution: (a) at the wall of the "Moby-Dick" nozzle straight section (Y=0.01065m), (b) at the throttle wall (Y=0.00017m) of the "Reitz" nozzle and (c) at the duct wall (X=0.038m) of the "Edwards' pipe" for t=0.3s.

3. Results

The numerical results as produced employing **Eqs. (2)-(4), (7) and (9)** are presented in a comparative manner in this section and validated against the available experimental data. The flow field emerging in the "Moby Dick" nozzle is illustrated through the contour plots of the pressure, velocity and temperature distributions in the throttle region (*0.4<X<0.64*) presented in **Fig. 4**. The predictions of the two-phase model employing the Hertz-Knudsen **Eq. (3)** for a λ value of *0.1* and the respective of HEM are indicatively shown in **Figs. 4a-f**, since, from a phase-change rate perspective, they correspond to thermodynamic non-equilibrium and equilibrium conditions, respectively. From a flow-topology point of view, it must be noted that the results produced using the other two-phase models considered (Knudsen, HRM and ZGB) bear resemblance to the ones shown in **Figs. 4a-c** referring to the Hertz-Knudsen model. The pressure contours shown in **Figs. 4a** and **4d** illustrate a considerable flow depressurization occurring downstream the nozzle throat. As can be also seen, the in-nozzle pressure values predicted by the HEM are higher in comparison to those produced by the Hertz-Knudsen model. This trend is attributed to the effect of the phase-change rate on the pressure distribution, as will be explained in more detail in the next paragraph referring to the Reitz case. The insets of **Figs. 4a** and **4d** elucidate that the pressure distribution obtains a minimal value at a location further downstream the nozzle throat, before adjusting to higher pressures, i.e. a shockwave is formed. Contours of the pressure-gradient magnitude are also depicted as black lines on the insets, in order to illustrate the formation of the shockwave, since, the gradient obtains large values at the location of formation. Both models predict the shockwave, however at non-coincident locations, since according to the HEM prediction, the shockwave forms approximately at X=0.82m, instead of X=0.67m as predicted by the Hertz-Knudsen model. **Figs 4b** and **4e**, depicting the velocity distribution, also reveal that the flow is accelerated at the divergent region, a clear indication of the expansion of initially under-expanded two-phase flow, which is associated with the

formation of a shockwave (Prudhomme and Haj-Hariri, 1994). The maximum velocity predicted by the HEM (**Fig. 4e**) in the expanding nozzle part is significantly higher than the respective of the two-phase, Hertz-Knudsen model (**Fig. 4b**), owing to the higher in-nozzle pressure predicted for equilibrium conditions, which leads to a more severe flow expansion downstream the nozzle throat. The Mach number distributions also depicted in **Figs. 4b** and **4d**, were calculated as the fraction of the mixture velocity to the respective local sonic velocity *c*, i.e. $M=u/c$. In the case of the HEM, where phase change is instantaneous and described through an EoS, the local sonic velocity is derived directly from the definition, i.e. $c^2 = \left(\frac{\partial p}{\partial \rho}\right)_s$, e.g. see Koop (2008):

$$\frac{1}{c_{mix}^2} = \frac{c_{v,mix}}{c_{p,mix}} \left(\frac{\partial \rho_{mix}}{\partial p}\right)_T \tag{11}$$

where $c_{v,mix}$ and $c_{p,mix}$ correspond to the specific heat at constant volume and pressure, respectively. For two-phase models, where, in concept, the mass-transfer rate is not "infinite", the following correlation, as suggested by Franc and Michel (2005) is implemented in Fluent (ANSYS FLUENT, 2012):

$$\frac{1}{\rho_{mix}\, c_{mix}^2} = \frac{a_v}{\rho_v\, c_v^2} + \frac{1-a_v}{\rho_l\, c_l^2} - \frac{\dot{R}}{\rho_v dp} \tag{12}$$

where c_l and c_v are the respective sonic velocities for the liquid and vapour phases, while the third term on the right hand side of the equation corresponds to the effect of phase-change on the mixture compressibility. As illustrated by the plots, the flow obtains sonic velocity (M=1) in the vicinity of the nozzle throat and further accelerates, thus becoming supersonic, at the divergent nozzle part. It must be noted that the sonic velocity that, in essence adjusts the flow velocity is different depending on the phase-change modelling approach, as it is designated by the local phase-field distribution. **Figs. 4c** and **4f** depicting the temperature field emerging at the throttle region and downstream verify this deduction, since the jet cooling predicted by the HEM is much more pronounced compared to the Hertz-Knudsen model, i.e. approximately 60K instead of 10K. The mixture temperature decreases due to the latent heat exchange required for bubble nucleation.

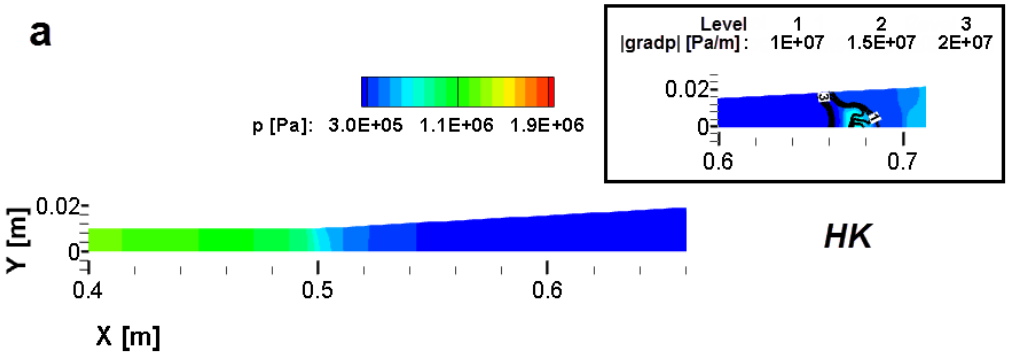

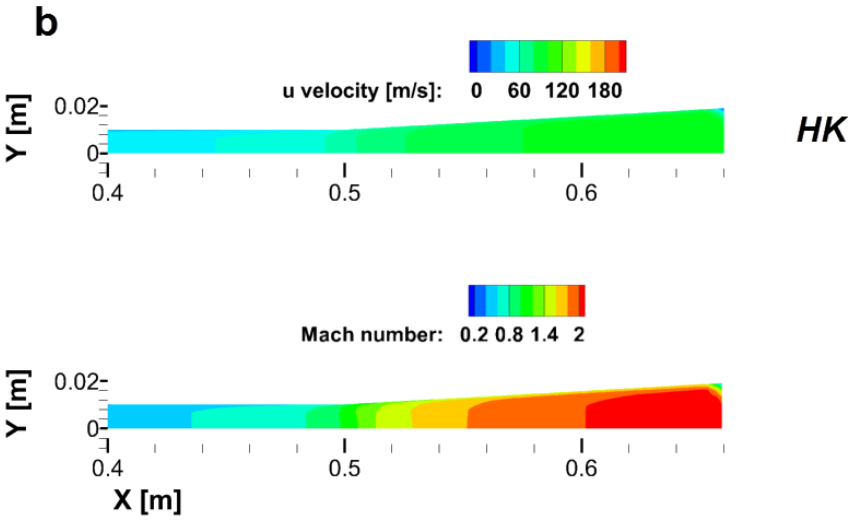
b
u velocity [m/s]: 0 60 120 180
Y [m]
0.02
0
0.4
0.5
0.6
HK
Mach number: 0.2 0.8 1.4 2
Y [m]
0.02
0
0.4
0.5
0.6
X [m]

555

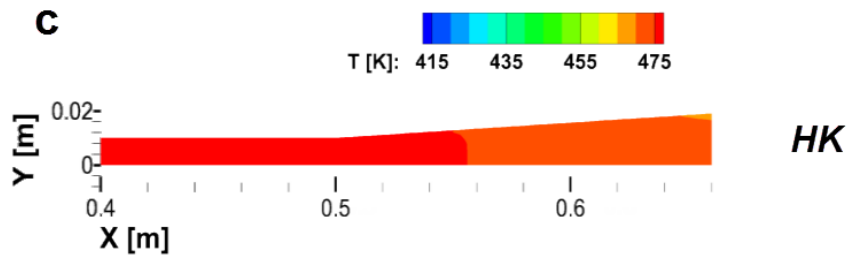
c
T [K]: 415 435 455 475
Y [m]
0.02
0
0.4
0.5
0.6
X [m]
HK

556

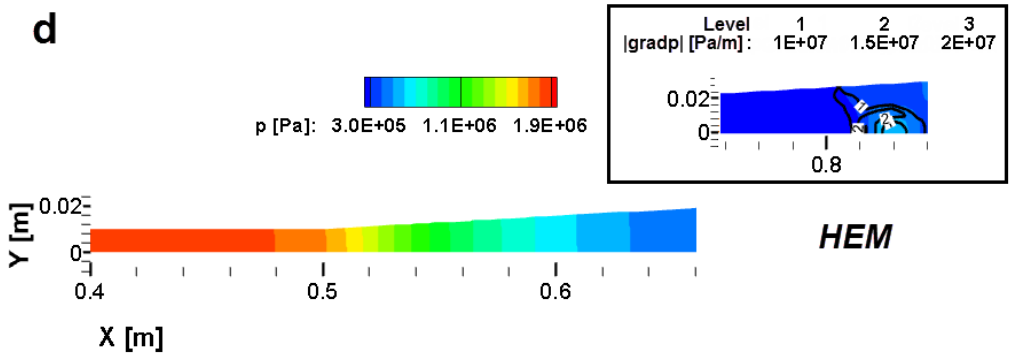
d
p [Pa]: 3.0E+05 1.1E+06 1.9E+06
Level 1 2 3
|gradp| [Pa/m]: 1E+07 1.5E+07 2E+07
0.02
0
0.8
Y [m]
0.02
0
0.4
0.5
0.6
X [m]
HEM

557

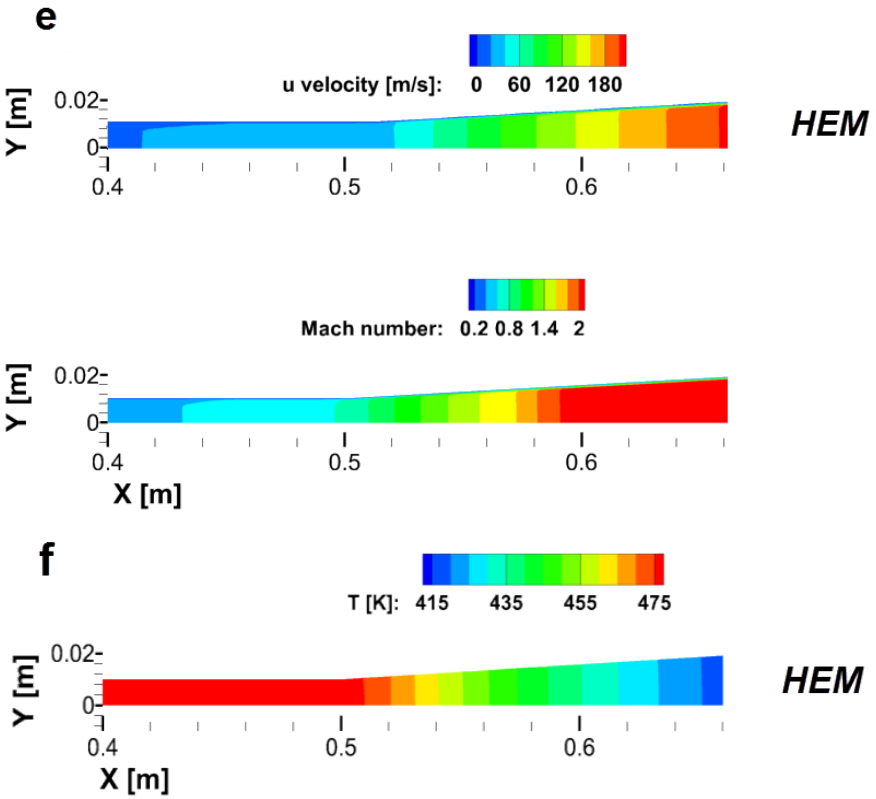

Figure 4. "Moby Dick" nozzle-Contour plots of (a, d) the pressure, (b, e) velocity and (c, f) temperature fields at the throttle region, as predicted using Hertz-Knudsen Eq. (3) for λ=0.1 (a-c) and HEM (d-f).

Fig. 5 depicts the pressure (**Fig. 5a**) and vapour volume fraction (**Fig. 5b**) distributions at the nozzle main axis. The comparison between the numerical predictions and the available experimental data of Asaka (1992) in reference to the pressure distribution illustrates that the models based on the kinetic theory of gases predict a more gradual liquid depressurization, compared to the HRM model with the closest agreement being accomplished for the predictions of the Knudsen model (**Eq. 2**). Referring to HRM, the pressure distribution produced using the "high-pressure" formulation exhibits higher values in the nozzle convergent part, which are in better matching with the experimental points, as expected since the inlet pressure is higher than 10 bar, compared to the predictions of the respective "low pressure" format. The discontinuity in the distribution observed at the divergent nozzle part ($X>0.65$) is associated with the shockwave formation due to flow expansion, as also illustrated in **Fig. 4a**. The ZGB model seems to be failing to predict both qualitatively and quantitatively the pressure drop within the nozzle, as the steep reduction predicted shows significant discrepancy to the experimental data.

The respective plot for the vapour volume fraction distribution (**Fig. 5b**) illustrates that almost full liquid vaporization has occurred at an axial distance of 0.65m. Adequate agreement exists between the predictions of all models and the experimental data. In fact, the closest matching to the experimental points is achieved by the predictions of the Hertz-Knudsen **Eq. (3)** for a value of the accommodation coefficient λ of 0.1, which suggests significant deviation from thermodynamic equilibrium. At this point, it must be highlighted that the ZGB model has been

significantly tuned, as the suggested value of 50 (Zwart et al., 2004) for the calibration coefficient F_e (see **Eq. 9**) produced a very steep phase-change process, highly deviating from the experimental data with almost full vaporization of the liquid at a location close to X=0.35. A sensitivity analysis was performed and a value of $F_e=3$ was eventually set, as it was found to produce results of acceptable agreement with the experimental data in reference to the vapour volume fraction distribution. This value ($F_e=3$) has been employed for all the test cases presented in this study. However, the model calibration (for $n_b=10^{13}$ m^{-3}) did not produce satisfactory results regarding the pressure distribution and further examination of the influence of the additional model coefficients (a_{nuc} and R_b), associated with the nucleation-site distribution, on the overall phase-change rate was deemed not to be within the scope of the present study. The specific model is oriented to cavitating flows and has been included in this investigation only as a reference, in order to confirm that, despite the similar macroscopic manifestation of the two phenomena, caution should be taken on the mechanism adopted for the modelling of the actual phase-change process.

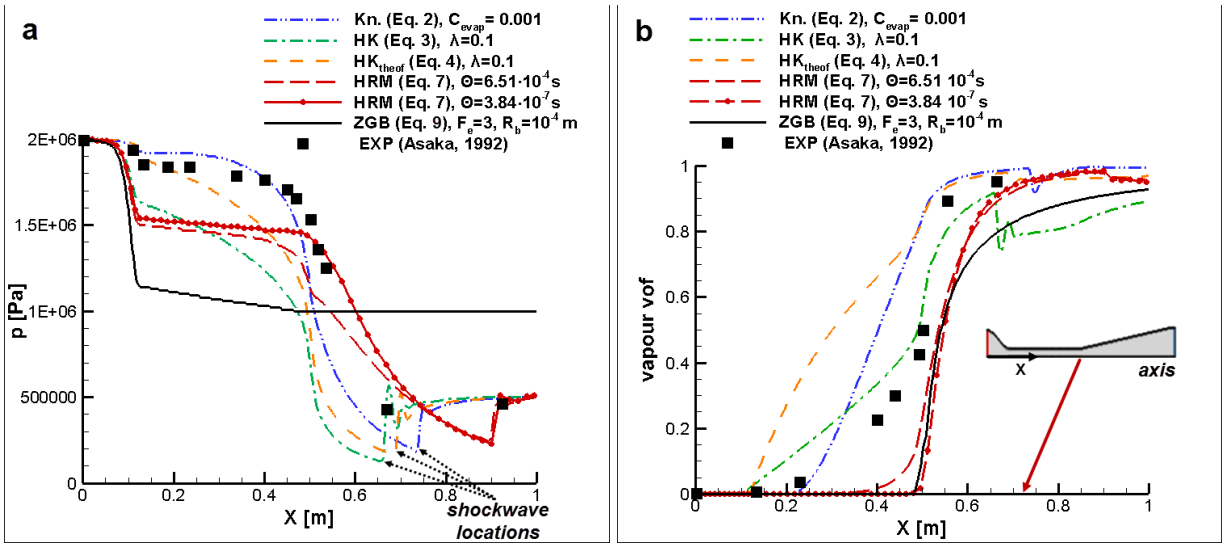

Figure 5. "Moby Dick" nozzle-Comparison of the numerical predictions to available experimental data: (a) Pressure and (b) vapour volume fraction at the axis along the nozzle length.

It must be pointed out that the predictions presented so far were produced considering a constant number of 10^{13} nucleation sites per unit volume. The effect of the nucleation-site density N_b on the numerical results is illustrated by **Fig. 6**, which depicts the predictions of the Hertz-Knudsen model (**Eq. 3**) for the "Moby Dick" case considering both constant and variable distributions of the nucleation-site density. In the latter case the distribution is correlated to the liquid superheat through **Eq. (10)**. The predictions based on a constant distribution of nucleation sites correspond to the dash-dot line of **Fig. 5** and have been added to **Fig. 6** as reference values. It can be clearly discerned in **Fig. 6a** that the pressure distribution predicted for $\lambda=1$, which corresponds to conditions close to thermodynamic equilibrium, and variable N_b exhibits an excellent agreement with the experimental data, while the respective distribution for $\lambda=0.1$ corresponds to a much more gradual pressure decrease at the throttle region. Likewise, as

depicted in **Fig. 6b**, the distribution of the vapour volume fraction for $\lambda=1.0$ and variable N_b, exhibits a very good match to the experimental data. The numerical predictions for the same case, as produced the HEM model are also depicted in **Fig. 6**. It is evident that the predictions of the equilibrium model, in which there are no considerations on nucleation sites but rather appropriate EoS are used, are in agreement with the respective of the Hertz-Knudsen model for λ=1. Hence, it can be deduced that the phase-change rate in the "Moby Dick" case is plausible to be corresponding to thermodynamic equilibrium. However, at this point it must be commented that the effects of these intrinsic two-phase flow features, i.e. activated nucleation-site distribution and prevailing thermodynamic conditions, are not distinguishable in a straightforward manner, since both lead to the augmentation of the overall phase change rate.

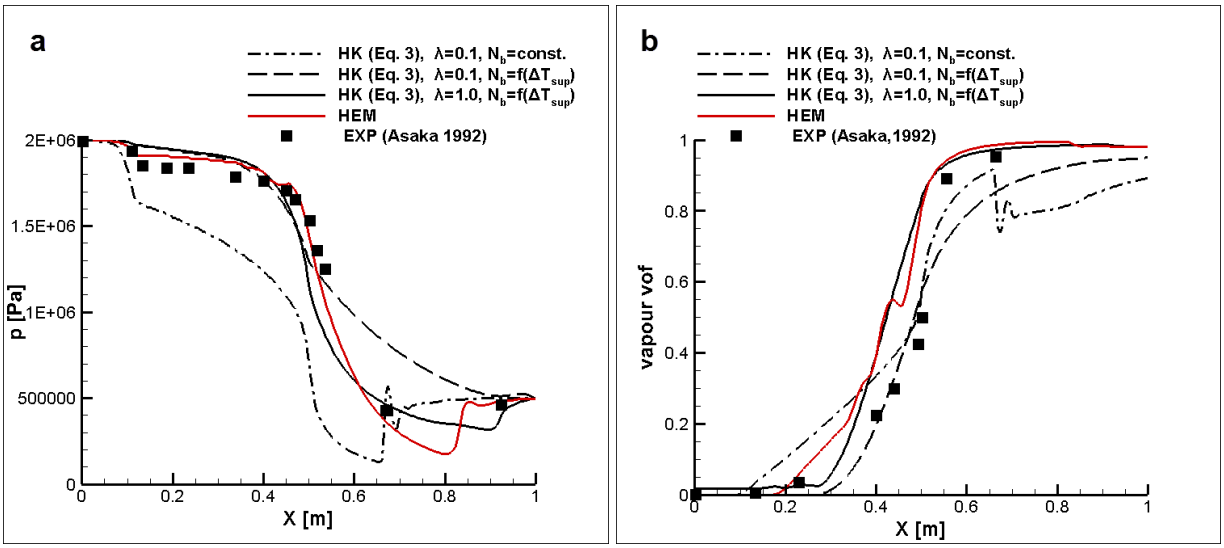

Figure 6. "Moby Dick" nozzle-Effect of the nucleation-site density distribution on the produced results: (a) pressure and (b) vapour volume fraction distribution.

Referring to the "Reitz" benchmark configuration, predictions of the phase field emerging within the nozzle are presented in **Fig. 7**. It can be clearly discerned that the bubble nucleation commences at the throttle vertex and gradually expands from the nozzle wall to the orifice axis. The low pressure at the throttle entrance due to flow separation at that region acts as the necessary perturbation for phase change to commence. Less extensive mass-transfer rate throughout the fluid bulk is predicted by the Hertz-Knudsen model, **Eq. (3)**, (**Fig. 7a**) compared to the HRM (**Fig. 7b**). The predictions of both models are in agreement with the qualitative findings of Reitz (1990), who reported that the liquid core could be discerned at the nozzle outlet and that severe atomization sets in immediately downstream the nozzle outlet. This "liquid core" is more pronounced in the predictions of the Hertz-Knudsen model, which in general predicts lower vapour volume-fraction values slightly downstream of the nozzle outlet compared to the HRM.

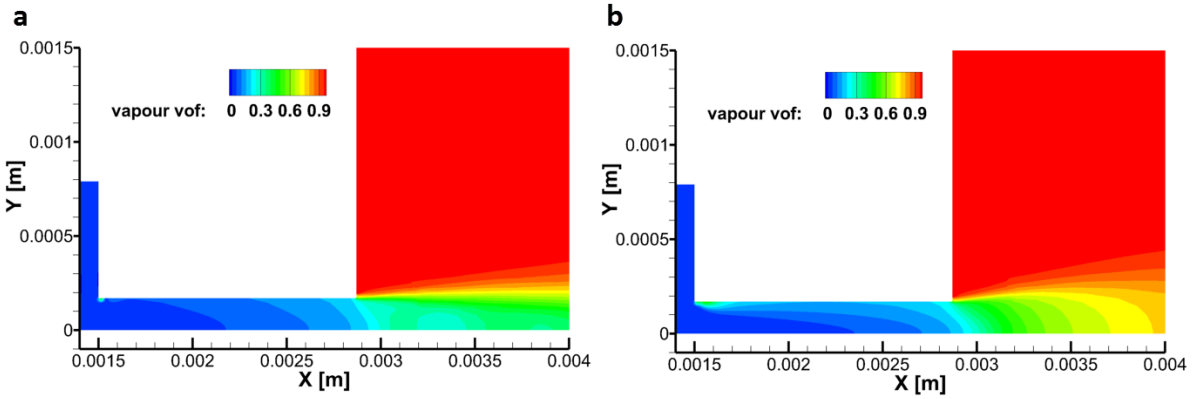

Figure 7. "Reitz" nozzle-Contour plots of the phase field for T=427K: (a) Hertz-Knudsen, Eq. (3) (λ=0.1), (b) HRM, Eq. (7) (Θ=6.51·10^{-4}s).

The pressure field in the "Reitz" nozzle as produced indicatively by the Hertz-Knudsen **Eq. (3)** and HRM**, Eq. (7)**, models is depicted in **Fig. 8.** As illustrated by both plots, a low pressure region sets in at the throttle entrance due to the flow separation. Further downstream, the flow retains relatively constant pressure values, while it drops to its atmospheric value in the vicinity of the nozzle outlet. The HRM model (**Fig. 8b)**, in general, predicts higher pressure values in the largest part of the throttle compared to the Hertz-Knudsen model (**Fig. 8a)**. As illustrated by the comparative plot of **Fig. 8c**, according to HRM results, pressure values are approximately 25% higher compared to the respective predictions based on the the Hertz-Knudsen model in a significant part of the throttle (*0.0018< X <0.0025*). This trend is associated with the higher mass-transfer rate predicted by the specific model (see **Fig. 7**), which, in turn, has a more considerable impact on the mixture compressibility in the nozzle region (Franc and Michel, 2005). The flow expansion downstream the injector outlet is associated with the formation of shockwaves, predicted by both models; the shockwave locations are signified by the low pressure regions downstream the outlet, as well as by the contours of the pressure-gradient magnitude, also plotted in **Figs. 8a-b** as black lines, which illustrate that significant flow depressurization occurs in the near-nozzle region. Further downstream, the pressure re-adjusts to the atmospheric value.

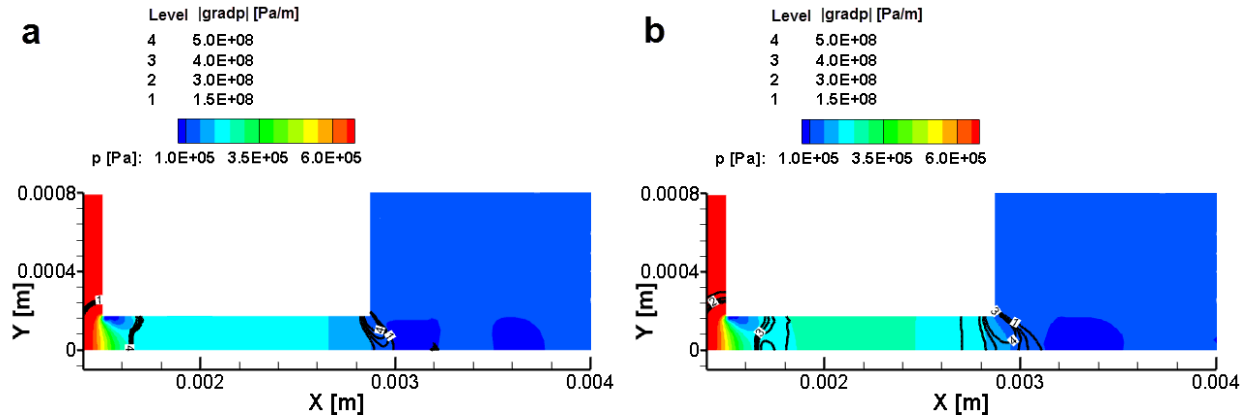

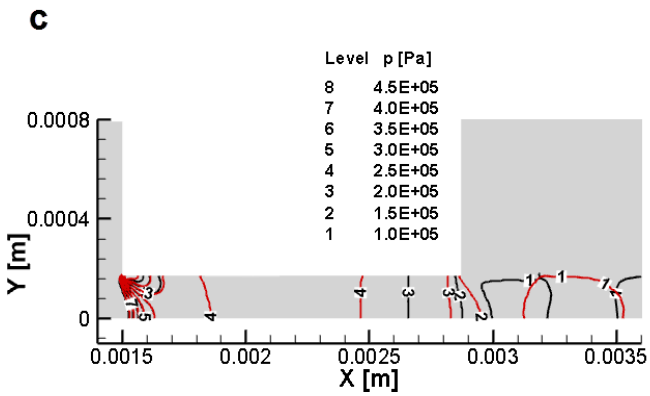

Figure 8. "Reitz" nozzle-Contour plots of the pressure field for T=427K: (a) Hertz-Knudsen, Eq. (3) (λ=0.1), (b) HRM, Eq. (7) ($\Theta=6.51\cdot10^{-4}$s) and (c) comparative contour plot with black and red lines corresponding to the predictions of HK and HRM, respectively.

Fig. 9a depicts the axial velocity distribution along the "Reitz" nozzle axis. It is evident that the flow is significantly accelerated as it enters the throttle region, where it subsequently retains relatively constant values. The Mach number ($M=u/c$) distribution for the two-phase mixture is also plotted on **Fig. 9a** and it illustrates that the flow velocity becomes equal to the speed-of-sound velocity c (M=1) at the outlet region, i.e. choked-flow conditions are reached. Downstream the outlet, the expansion of the two-phase mixture constitutes the flow supersonic, with the predicted Mach numbers being in the range 1.7-2.4. The predictions of the three models depicted in **Fig. 9a** have a similar form with the Knudsen mass-transfer model predicting a slightly higher acceleration downstream of the nozzle outlet.

The effect of the liquid temperature on the mass flow rate through the nozzle inlet is depicted in **Fig. 9b**. As can be seen, the flow rate is decreased by approximately 10% in the temperature range considered 400-427K as the extent of the nozzle cross-sectional area occupied by vapour increases due to the increased phase-change rate and thus the available active area for the liquid to flow decreases. The predictions of all models are in good agreement with the experimental data available by Reitz (1990) and the minor flow-rate decrease is well captured by all models. The calibrated ZGB model is in the specific case seems capable of capturing a macroscopic flow features, such as the overall mass-flow rate. Besides, it must be noted that numerical results shown in **Fig. 9b** correspond to low-phase change rate indicative of non-equilibrium conditions (Koukouvinis et al., 2016). A parametric study was conducted, so as to further verify that the thermodynamic conditions in reference to the "Reitz" case correspond to non-equilibrium. The case for T=427K was considered and the numerical predictions produced by the Hertz-Knudsen model, Eq. (3), for different combinations of λ and n_0 were compared against the experimental value for the inlet mass flow rate. As can be deduced from the values of **Table 1,** the closest agreement to the experiment is accomplished for the set of parameters selected for the production of the results presented in **Figs. 7-9**, i.e. $n_0=10^{13}$ and λ=0.1. Increasing the λ value to 1 leads to the prediction of significantly lower mass-flow rate due to the enhanced in-nozzle phase-change rate, while the discrepancy from the experimental value is increased. This signifies that the flow conditions in the "Reitz case" are characterized by a strong deviation from thermodynamic equilibrium.

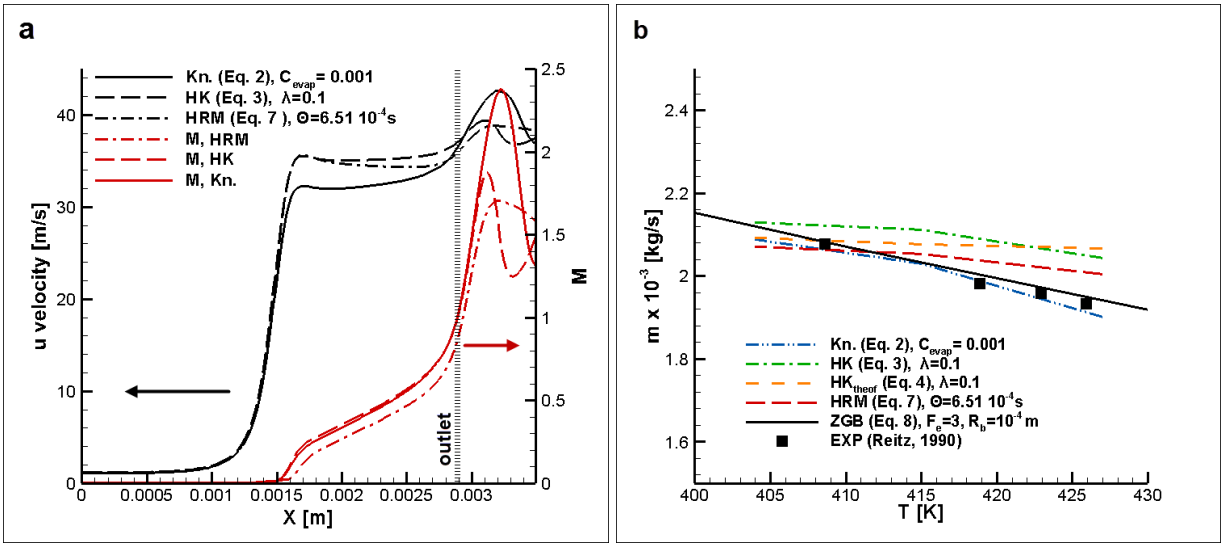

Figure 9. "Reitz" nozzle: (a) Velocity and Mach number distributions at the nozzle axis and (b) mass-flow rate at the nozzle inlet.

Table 1. Predictions of the Hertz-Knudsen model for different λ and n_0 values.

λ	n_0 [m^{-3}]	$\dot{m}$ [g/s]	Deviation (%)
0.1	const. (=10^{13})	2.043	5.68
1.0	const. (=10^{13})	1.662	14.02
0.1	$f(\Delta T_{sup})$ Eq. (10)	2.097	8.50
1.0	$f(\Delta T_{sup})$ Eq. (10)	1.747	9.60

The pressure and vapour volume fraction distributions at the axis of the "Edwards' pipe", the third benchmark geometry examined in this study, are depicted for different time instances in **Fig. 10**. As made evident by **Fig. 10a,** a rarefaction wave propagates with the speed of sound of the liquid phase into the pipe. The pressure continues to drop, until atmospheric conditions prevail throughout its entire volume at approximately 0.5s. **Fig. 10b** illustrates that phase change commences exactly at the pipe outlet and the vaporization front travels upstream towards the inlet, as indicated by the line corresponding to t=0.1s. Almost full liquid vaporization has occurred after 0.5s from the beginning of the transient flow process.

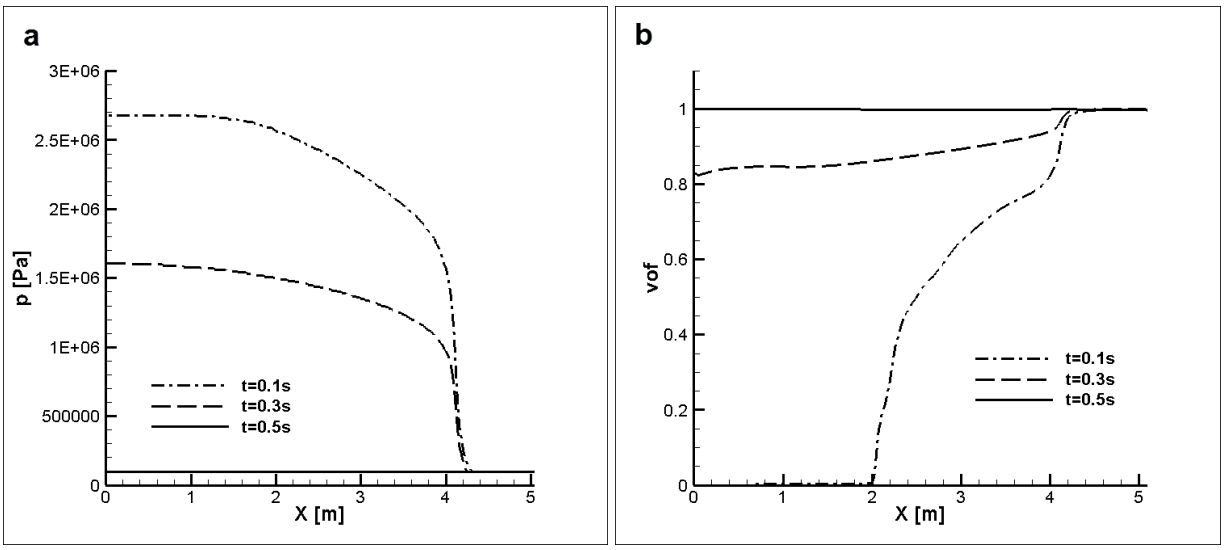

Figure 10. Edwards' (a) Pressure and (b) vapour volume fraction distributions at the duct axis for various time instances (Hertz-Knudsen Eq. (3), λ=0.1): (a) t=0.1s, (b) t=0.3s and (c) t=0.4s.

The temporal evolution of the velocity field is illustrated by the contour plots of **Fig. 11**. As can be seen, the flow is significantly accelerated towards the pipe outlet and the two-phase jet is expelled to ambient with an increased cone angle. The increased cone angle is once again due to the expansion of the mixture fluid downstream the nozzle outlet. The detailed view of the Mach number distribution in the vicinity of the duct outlet, also depicted in **Fig. 11**, confirms that the flow is choked (Mach number equal to unity) for all time instances shown and that the two-phase mixture expands to supersonic flow further downstream. As the phenomenon evolves and hence the vaporization front reaches closer to the pipe left end, the local velocity in the vicinity of the outlet, which is adjusted by the local phase field, increases from approximately 80m/s at t=0.1s (**Fig. 11a**) to 180m/s at t=0.4 (**Fig. 11c**), while at the same time the downstream region of elevated velocities is reduced. It must be highlighted that the flow remains choked even for t=0.4s, however the downstream expansion is less pronounced compared, e.g., to t=0.1s. Hence, it is logical to deduce that as the local mixture quality at the outlet approaches pure vapour, the local speed-of-sound velocity, which adjusts the flow velocity in the duct, increases and consequently the flow expansion becomes less violent.

736

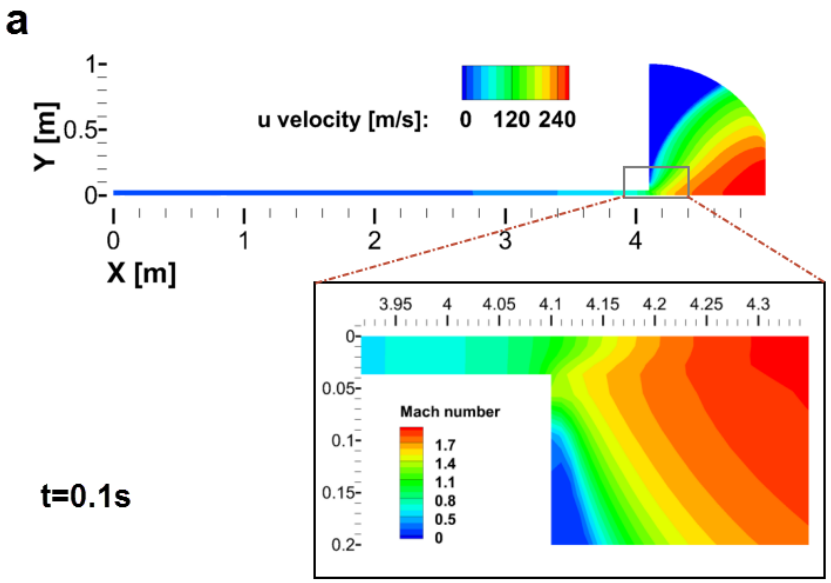
a
u velocity [m/s]: 0 120 240
Y [m]
X [m]
Mach number
1.7
1.4
1.1
0.8
0.5
0
t=0.1s

737

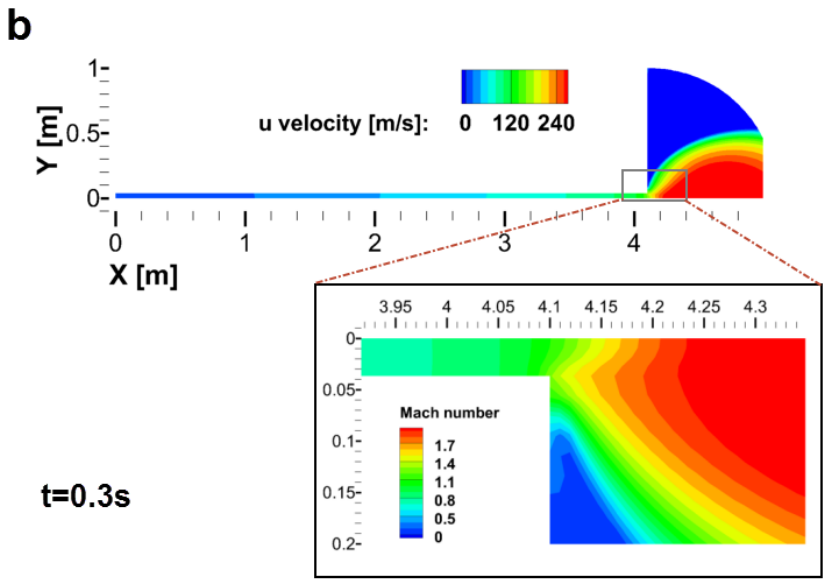
b
u velocity [m/s]: 0 120 240
Y [m]
X [m]
Mach number
1.7
1.4
1.1
0.8
0.5
0
t=0.3s

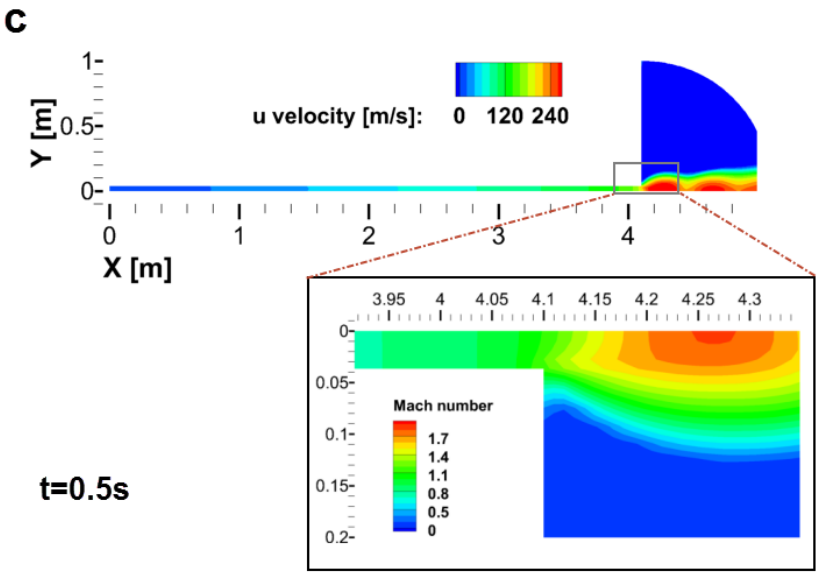

Figure 11. "Edwards' pipe"-Contour plots depicting time instances of the velocity field (Hertz-Knudsen **Eq. 3**, λ=0.1): t=0.1s, (b) t=0.3s and (c) t=0.4s.

Fig. 12 depicts the comparison between the predictions of four two-phase models, namely **Eqs. (2)-(4)** and **(7)** and the experimental data available by Edwards and O'Brien (1970) regarding the time evolution of the pressure at the pipe head and the vapour volume fraction at the pipe mid-section. It was decided the ZGB not to be tested in the present case, since its formulation has not been suggested for cases where mass-transfer occurs through a single interphase, as in the "Edwards' pipe" case. As can be seen the Knudsen and Hertz-Knudsen **Eqs. (2)-(4)** considering a λ value of 0.1 produce accurate predictions regarding both pressure (**Fig. 12a**) and vapour volume fraction (**Fig. 12b**). Specifically referring to the volume fraction distribution, it has to be commented that, as can be seen on **Fig. 12b,** the first two experimental points cannot be captured by the Hertz-Knudsen models. However, failure of the models to accurately capture the phase field should also reflect to their predictions regarding the pressure field, since the mass-transfer rate affects the mixture compressibility, as has been pointed out in the previous paragraphs. Yet the predictions are in agreement to the experimental data with regard to pressure. Furthermore, the working medium has not been characterized in terms of gas content or impurities and the experimental uncertainties associated with the data have not been reported and thus the possibility of non-condensable gas effects to be responsible for the discrepancy detected cannot be assessed. Gas bubbles serving as nucleation sites should be expected to enhance the vaporization rate throughout the evolution of the phenomenon and hence the discrepancy between experimental data and numerical prediction should ensue for all time instances. For low vapour-fraction values in the order of 15%, more plausible explanations for the deviation are considered the relatively high experimental error associated with such values, which correspond to low signal to noise ratio for the measuring sensor, or possible density fluctuations that are recorded as vapour generation (see Mauger et al., 2012). Hence, the predictions validity of the models based on the kinetic theory of gases regarding flashing flows can be considered to have been verified for all the flow configurations examined in the present investigation.

The "high pressure" formulation of the HRM was deemed as suitable for predicting the flow in the "Edwards pipe" case, in which the initial pressure substantially exceeds 20 bar. The respective results, also depicted on **Fig. 12** demonstrate that the flow can be qualitatively captured in terms of both the pressure and vapour volume fraction distribution, however a more significant depressurization is predicted by the model compared to the experimental data (**Fig. 12a**) and this is attributed to the lower mass-transfer rate predicted (**Fig. 12b**), as has been already discussed in the previous paragraphs of this section. The quantitative deviation between the HRM predictions and the experiment is probable to stem from the semi-empirical parameters associated with the model, since their values have been determined considering steady, inlet-outlet flows with distinct differences from this case.

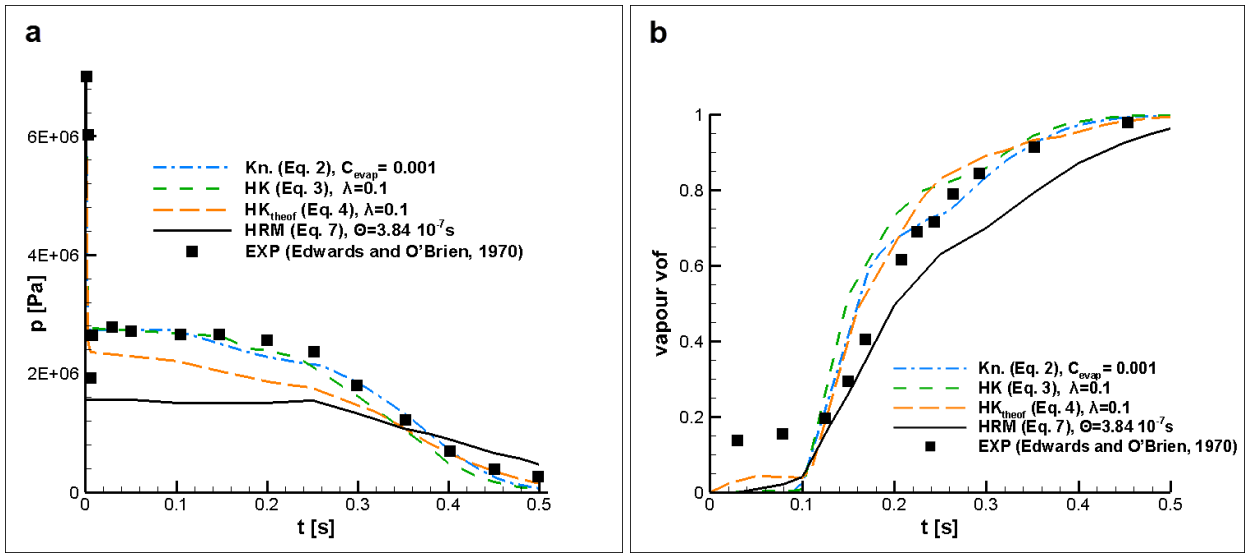

Figure 12. "Edwards' pipe"-Comparison of the numerical predictions to experimental data: (a) pressure at the pipe (left) outer wall, (b) vapour volume fraction at the pipe mid-section.

4. Conclusions

Different two-phase, mass-transfer models based on fundamental concepts such as the kinetic theory of gases, thermodynamic non-equilibrium and bubble-dynamics considerations, as well as a homogeneous equilibrium model, have been evaluated in a comparative manner in the present numerical investigation. The models based on the kinetic theory of gases, were found to produce accurate predictions regarding all the benchmark geometries considered, while the HRM model was also capable of capturing the two-phase flow in all cases, yet producing results with higher discrepancy to the experiment compared to Knudsen and Hertz-Knudsen mechanisms. On the contrary, the applicability of ZGB model was demonstrated to be doubtful. Especially regarding the ZGB model, which has been formulated for the prediction of cavitating flows, the phase-change rate that results if the standard model coefficient values are used is much higher than the one indicated by the experimental data. Therefore, although the two phenomena, i.e. cavitation and flash boiling macroscopically may seem as similar, it has been confirmed that the underlying phase-change mechanisms are of different nature.

The numerical results were demonstrated to be highly sensitive to the distribution of the activated nucleation sites, which has a significant influence on the overall phase-change process and its accurate determination is a prerequisite conditions prior to making any deductions in reference to the deviation of the flashing flow from thermodynamic-equilibrium conditions. Besides, the effects of the bubble-growth mechanism and the nucleation-site density on the overall phase change rate cannot be distinguished, since they both act in an enhancive manner. Referring to the flow phenomena associated with the onset of flash boiling conditions, it was verified through the numerical predictions that the phase and velocity fields are strongly linked, as the local speed-of-sound velocity is designated by the quality of the liquid/vapour mixture and, in turn, limits the local flow velocity. Flow choking due to effect of phase change takes place at the location of the geometrical constriction followed by expansion in the diverging part of the geometry, increase of the jet cone angle and formation of shockwaves in the vicinity of the outlet region. Flow expansion has been found to be linked to enhanced spray atomization and therefore the next step of future research will be to utilize the validated models in simulations of realistic fuel injector configurations.

Acknowledgements

The research leading to these results has received funding from the People Programme (IAPP Marie Curie Actions) of the European Union's Seventh Framework Programme FP7/2007-2013/ under REA grant agreement n. 324313.

References

ANSYS FLUENT, 2012, *Theory Guide V14.5*, p. 724–746.

Aleiferis, P. G., and Van Romunde, Z. R. 2013. An Analysis of Spray Development with Iso-Octane, N-Pentane, Gasoline, Ethanol and N-Butanol from a Multi-Hole Injector under Hot Fuel Conditions. Fuel. 105, 143–168.

Araneo, L., Coghe, A., Brunello, G. and Donde, R. 2000. Effects of Fuel Temperature and Ambient Pressure on a GDI Swirled Injector Spray. SAE Tech. papers 724, 2000-01-1901.

Asaka, A. 1992. CATHARE – Qualification of Critical Flow Experiments. Centre d'Etudes Nucleaires de Grenoble, report STR/LML/EM/92-108.

Battistoni, M., Som, S., and Longman, D. E. 2014. Comparison of Mixture and Multifluid Models for In-Nozzle Cavitation Prediction. J. Eng. Gas Turb. Power, 136, 061506.

Bilicki, Z., and Kestin, J. 1990. Physical Aspects of the Relaxation Model in Two-Phase Flow. Proc. R. Soc. London A. 428, 379–397.

Brennen, C.E. 1995. Cavitation and Bubble Dynamics. Oxford University Press, Available at http://authors.library.caltech.edu/25017/1/cavbubdynam.pdf.

Chan, Q. N., Bao, Y., and Kook, S. 2014. Effects of Injection Pressure on the Structural Transformation of Flash-Boiling Sprays of Gasoline and Ethanol in a Spark-Ignition Direct-Injection SIDI Engine. Fuel. 130, 228–240.

Chen, Z.J. and Przekwas, A.J. 2010. A Coupled Pressure-Based Computational Method for Incompressible /Compressible Flows. J. Comp. Phys., 229, 9150–9165.

Demirdžić, I., Lilek, Ž. and Perić, M. 1993. A Collocated Finite Volume Method for Predicting Flows at all Speeds. Int. J. Numer. Meth. Fluids, 16, 1029–1050.

Edwards, A. R., and O'Brien, T. P. 1970. Studies of Phenomena Connected with the Depressurization of Water Reactors. J. Brit. Nucl. En. Soc. 9, 125–135.

Engine Combustion Network. 2014. "Spray G" Operating Conditions. Sandia National Laboratories, Livermore, CA.

Franc, J.P. and Michel, J.M. 2005. Fundamentals of Cavitation. Kluwer Academic Publishers, New York, p. 165-168.

Fuster, D., Hauke, G., Dopazo, C. 2010. Influence of the Accommodation Coefficient on Nonlinear Bubble Oscillations. J. Acoust. Soc. America. 128, 5-10.

Gopalakrishnan, S. and Schmidt, D.P. 2008. Multidimensional Simulation of Flash-Boiling Fuels in Injector Nozzles. Proc. Am. Conf. Liquid Atomiz. Spray Syst.

Janet, J.P., Liao, Y. and Lucas, D. 2015. Heterogeneous Nucleation in CFD Simulation of Flashing Flows in Converging–Diverging Nozzles. Int. J. Multiph. Flow, 74, 106–117.

Ji, B., Luo, X., Arndt, R.E.A. and Wu, Y. 2014. Numerical Simulation of Three Dimensional Cavitation Shedding Dynamics with Special Emphasis on Cavitation–Vortex Interaction, Ocean Eng., 87, 64–77.

Karathanassis, I. K., Koukouvinis, P. and Gavaises, M. 2016. Topology and distinct features of flashing flow in an injector nozzle. Atomiz. Sprays. 26, 1307-1336.

Knudsen, M. 1915. Die maximale Verdampfungsgeschwindigkeit des Quecksilbers. An. Phys. 352, 697–708.

Koop, A. H. 2008. Numerical Simulation of Unsteady Three-Dimensional Sheet Cavitation. PhD thesis. University of Twente.

Koukouvinis, P. and Gavaises, M. 2015. Simulation of Throttle Flow with Two Phase and Single Phase Homogenous Equilibrium Model. J. Phys.: Conf. Series, 656, 012086.

Koukouvinis, P., Naseri, H. and Gavaises, M. 2016. Performance of Turbulence and Cavitation Models in Prediction of Incipient and Developed Cavitation. Int. J. Engine Res, 17, 1–18.

Lamanna, G., Kamoun, H., Weigand, B., and Steelant, J. 2014. Towards a Unified Treatment of Fully Flashing Sprays. Int. J. Multiph. Flow. 58, 168–184.

Lee, J., Madabhushi, R., Fotache, C., Gopalakrishnan, S., and Schmidt, D. 2009. Flashing Flow of Superheated Jet Fuel, Proc. Combust. Inst. 32, 3215–3222.

870 Liao, Y., Lucas, D. 2015. 3D CFD Simulation of Flashing Flows in a Converging-Diverging Nozzle.
871 Nucl. Eng. 292, 149-163.

872 Magnini, M. and Pulvirenti, B. 2011. Height Function Interface Reconstruction Algorithm for the
873 Simulation of Boiling Flows, in Mammoli, A.A., and Brebbia, C.A. "Computational Methods in
874 Multiphase Flow VI", WIT press, UK, 69-80.

875 Mauger, C., Méès, L., Michard M., Azouzi, A. and Valette, S. 2012. Shadowgraph, Schlieren and
876 Interferometry in a 2D Cavitating Channel Flow. Exp. Fluids, 53, 1895–1913.

877 Menter, F.R. Best Practice: Scale-Resolving Simulations in ANSYS CFD. ANSYS Germany GmbH,
878 2012

879 Mojtabi, M., Chadwick, N., Wigley, G., and Helie, J. 2008. The Effect of Flash Boiling on Break up and
880 Atomization in GDI Sprays. Proc. 22nd Euro. Conf. Liquid Atomiz. Spray Syst.

881 Neroorkar, K., Gopalakrishnan, S., Grover, Jr., R. O., Schmidt, D. P. 2011. Simulation of Flash Boiling in
882 Pressure Swirl Injectors. Atomiz. Sprays. 21, 179–188.

883 Oza, R. D. 1984. On the Mechanism of Flashing Injection of Initially Subcooled Fuels. J. Fluids Eng.
884 106, 105-109.

885 Payri, F., Pastor, J. V, Pastor, J. M. and Juliá, J. E. 2006. Diesel Spray Analysis by Means of Planar
886 Laser-Induced Exciplex Fluorescence. Int. J. Engine Res. 7, 77–89.

887 Price, C., Hamzehloo, A., Aleiferis, P. and Richardson, D. 2015. Aspects of Numerical Modelling of
888 Flash-Boiling Fuel Sprays Flash-Boiling Atomization. SAE Tech. Pap. 2015-24-2463.

889 Prudhomme, S.M. and Haj-Hariri, H. 1994. Investigation of Supersonic Underexpanded Jets using
890 Adaptive Unstructured Finite Elements. Fin. Elem. Anal. Design. 17, 21-40.

891 Reitz, R. D. 1990. A Photographic Study of Flash-Boiling Atomization. Aerosol Sci. Technol. 12, 561–
892 569.

893 Riznic, J. R. and Ishii M. 1989. Bubble Number Density and Vapor Generation in Flashing Flow. Int. J.
894 Heat Mass Transf. 32, 1821–1833.

895 Saha, K., Som, S., Battistoni, M., Li, Y., Quan, S., and Senecal, P. K. 2016. Modeling of Internal and
896 Near Nozzle Flow for a Gasoline Direct Injection Fuel Injector, *J. En. Res. Tech*. 138, 052208-1.

897 Sens, M., Maass, J., Wirths, S. and Marohn, R. 2012. Effects of Highly-Heated Fuel and / or High
898 Injection Pressures on the Spray Formation of Gasoline Direct Injection Injectors. Fuel Systems for IC
899 Engines, Woodhead Publishing.

900 Schmidt D.P., Gopalakrishnan. H. and Jasak, H. 2010. Multi-dimensional Simulation of Thermal Non-
901 equilibrium Channel Flow. Int. J. Multiph. Flows, 36, 284-292.

902 Senda, J. and Hojyo, Y. 1994. Modeling on Atomization and Vaporization Process in Flash Boiling
903 Spray, JSAE Review, 15, 291–296.

Serras-Pereira, J., Van Romunde, Z., Aleiferis, P.G., Richardson, D., Wallace, S. and Cracknell, R.F. 2010. Cavitation, Primary Break-up and Flash Boiling of Gasoline, iso-Octane and n-Pentane with a Real-size Optical Direct-Injection Nozzle. Fuel. 89, 2592–2607.

Shin, T. S., and Jones, O. C. 1993. Nucleation and Flashing in Nozzles-A distributed Nucleation Model. Int. J. Multiphase Flow. 19, 943–964.

Singhal, A.K., Athavale, M.M., Li, H., and Jiang, Y. 2002. Mathematical Basis and Validation of the Full Cavitation Model. J. Fluids Eng. 124, 617-624.

Staedtke, H. 2006. Gasdynamic Aspects of Two-Phase Flow. Wiley VCH, Weinheim, 59-71.

Theofanous, T., Biasi, L., Isbin, H. S. and Fauske, H. 1969. A Theoretical Study on Bubble Growth in Constant and Time-Dependent Pressure Fields. Chem. Eng. Sci. 24, 885–897.

Vieira, M.M. and Simões-Moreira, J.R. 2007. Low-Pressure Flashing Mechanisms in iso-Octane Liquid Jets. J. Fluid Mech. 572, 121-144.

Wagner, W., and Pruss, A. 2002. The IAPWS Formulation 1995 for the Thermodynamic Properties of Ordinary Water Substance for General and Scientific Use. J. Phys. Chem. Ref. Data. 31, 387-535.

Yuan, W., Sauer, J., and Schnerr, G.H. 2001. Modeling and Computation of Unsteady Cavitation Flows in Injection Nozzles, Mec. Ind., 2, 383–394.

Zeng, W., Xu, M., Zhang, G., Zhang, Y., and Cleary, D. J. 2012. Atomization and Vaporization for Flash-boiling Multi-hole Sprays with Alcohol Fuels. Fuel. 95, 287–297.

Zhang, G., Xu, M., Zhang, Y., Zhang, M. and Cleary, D. J. 2013. Macroscopic Characterization of Flash-Boiling Multihole Sprays Using Planar Laser-Induced Exciplex Fluorescence. Part II, Cross-Sectional Spray Structure. Atomiz. Sprays, 23, 265–278.

Žnidarčič, A., Mettin, R. and Dular, M. 2015. Modeling Cavitation in a Rapidly Changing Pressure Field – Application to a Small Ultrasonic Horn, Ultrason. Sonochem., 22, 482-92.

Zuo, B., Gomes, A. M. and Rutland, C. J. 2000. Modelling Superheated Fuel Sprays and Vaporization, Int. J. Eng. Res., 1, 321–336.

Zwart, P.J., Gerber, A.G. and Belamri, T. 2004. A Two-Phase Flow Model for Predicting Cavitation Dynamics, Proc. of 5th Int. Conf. on Multiph. Flow.